A Control Plan for the Stable Operation of Microgrids during Grid-connected and Islanded Modes

Majid Mehrasa [a], Edris Pouresmaeil [b], Bo Nørregaard Jørgensen [b], and João P. S. Catalão [c,d,e]

[a] Young Researchers and Elite Club, Sari Branch, Islamic Azad University, Sari, Iran
[b] Centre for Energy Informatics, University Of Southern Denmark, Odense, Denmark
[c] University of Beira Interior, R. Fonte do Lameiro, Covilha, Portugal
[d] INESC-ID, R. Alves Redol, Lisbon, Portugal
[e] IST, University of Lisbon, Av. Rovisco Pais, Lisbon, Portugal

I. Nomenclature

Indices

i	1,2
k	a,b,c
z	d,q

Variables

i_{cki}	DG current components in abc frame
v_{dci}	dc-link voltage
i_{fki}	Currents of filter capacitors in abc frame
v_k	Voltage at the PCC in abc frame
s_{ki}	Switching functions of DG units
u_{eqki}	Equivalent Switching function of DG units
i_{czi}	DG current components in dq frame
v_{zi}	Voltage at the PCC in dq frame
i_{fzi}	Currents of filter capacitors in dq frame
u_{eqzi}	Equivalent Switching function of DG units
i^*_{czi}	Reference current components of DG units
$\tilde{I}_{av_d}, \tilde{I}_{av_q}$	Average values of reference currents
f_i^*	Reference frequency of DG unit
E_i	Amplitude of voltages at PCC
E_i^*	Reference amplitude of PCC voltages
Δf_i	Frequency variation of DG units
ΔE_i	Variation of voltage amplitudes at the PCC
U_{eqzi}	Dynamic state switching function
i_{llz}	Local Load currents in dq frame
i_{mlz}	Main Load current in dq frame
I_{lld1}	d-component of Local Load current in main frequency
u^*_{eqzi}	Reference switching function of DG units
v^*_{dci}	Reference voltage of dc-link
v_{mi}	Maximum voltage amplitude at the PCC
i^*_{fzi}	Reference currents of filter capacitors
i^*_{dci}	Reference current of dc-link
I^*_{avzi}	Average values of reference currents of DG
P_{DGi}	DG active power
Q_{DGi}	DG reactive power
$\tilde{i}_{czi}$	Average value of current in DG units
$\tilde{v}_{dci}$	Average value of dc-link voltage
$P_{DGi\max}$	Maximum active power of DG units
$Q_{DGi\max}$	Maximum reactive power of DG units
P^*_{DGi}	Reference active power of DG units
Q^*_{DGi}	Reference reactive power of DG units
ΔP_{DGi}	Variation of active power in DG units
ΔQ_{DGi}	Variation of reactive power in DG units
$\tilde{i}_{lld}$	Harmonic current components of Local Load
$\tilde{i}_{mld}$	Harmonic current component of Main Load

Parameters

L_{sm}	Machine Inductance
R_{sm}	Machine Resistance
r	Rotor Radius
A	Wind Turbine Rotor Swept Area
ρ	Air Density
R_g	Resistance of utility grid
L_g	Inductance of utility grid

Corresponding Author: João P. S. Catalão, Email: catalao@ubi.pt
Tel: +351-275-329914; Fax: +351-275-329972.

I_{mld1}	d-component of Main Load current in main frequency	R_{ci}	Resistance of DG unit
m	Slope of $P-f$ curve	L_{ci}	Inductance of DG unit
n	Slope of $Q-E$ curve	C_{dci}	Capacitor of DG unit
P_{mech}	Output Mechanical Power	C_{fi}	Capacitor of filter
C_p	Power Coefficient	ω	Grid angular frequency
λ	Tip Speed Ratio	(α_i, β_i)	Constant coefficients for the dynamic state switching functions
β	Blade Angle	***Abbreviation***	
U_m	Wind Speed	WTS	Wind Turbine System
ω_m	Mechanical Angular Velocity of Generator	DG	Distributed Generation
v_{zm}	Machine Voltages in d-q frame	SVPWM	Space Vector Pulse Width Modulation
		PCC	Point of Common Coupling
λ_m	Flux Linkage Amplitude	S	Switch
		CHP	Combined Heat and Power
ω_r	Angular Frequency of the Stator Voltage	CC	Capacity Curve
		VSI	Voltage Source Inverter
V_z	Reference Synchrony Frame Voltages	DLCM	Direct Lyapunov Control Method
		LPF	Low Pass Filter
$i^*_{h1_{di}}$	Completing d-Component Reference Current	PMSG	permanent magnet synchronous generator
		PI	Proportional-Integral
T_e	Electromagnetic Torque		

***Abstract*—This paper presents a control technique that enhances microgrids stability during the grid-connected and islanded modes. The proposed technique is compared with several existing control strategies in the context of microgrids integration into smart grids. The Lyapunov control theory is utilized in this paper to investigate the operation stability of DG units operating along with the utility grid. As the main contribution, the proposed technique compensates for the instantaneous variations of the reference current components of DG units in the *ac*-side of the converters. The presented method also considers and properly addresses the *dc*-voltage variations in the *dc*-side of the interfacing system. Under the proposed control strategy, DG units are able to deliver active and reactive power to the local loads and/or the main grid in fundamental and harmonic frequencies, with a fast dynamic response and without any interruption. Several simulation scenarios are carried out to demonstrate effectiveness of the proposed control strategy in microgrids during the transient and steady-state operation.**

***Index Terms*—Microgrid; distributed generation (DG); grid-connected mode; islanded mode; voltage source inverter (VSI); Lyapunov control theory.**

II. Introduction

The renewable energy sources integration in the form of distributed generation (DG) provides several benefits for the utility grid considering the environmental regulations and the cost of power generation [1]. Integration of DG units into the main power grid can improve the power quality and increase the reliability of the electricity supply by mitigating the problems associated with the peak demand loads and the grid failure. Compared to individually operated DGs, a systematic integration of DG units, in the form of a microgrid, can further increase the grid reliability and power quality [2-3].

A microgrid can operate either in the grid-connected or islanded mode; for each operation mode, several control techniques have been developed to perform active and reactive power sharing as well as frequency and voltage regulation [4, 5], such as potential-function based method for secondary and tertiary control of a microgrid [6], unit output power control (UPC) and feeder flow control (FFC) [7], power management strategies [8], droop-control concepts with L_1 control theory [9], and other proposed control strategies [10-12].

In [13], two distinct strategies are discussed for controlling the active power and frequency of multiple DG units in a microgrid. Another control strategy is proposed in [14] for the integration of microgrids into the main power grid, and a voltage-control technique is presented in [15]. In [16], a power control and sharing technique is discussed for the electronically coupled DG units, in which the output active and reactive power of DG units can be properly controlled in both the islanded and grid-connected modes. A two-degree-of-freedom (DOF) controller is utilized for a DG-based system as an uninterruptible power supply (UPS) to keep the voltage of AC bus at the desired value in presence of the stochastic behaviour of the loads [17]; this proposed DG model demonstrates a smooth transition from the grid-connected mode to the islanded mode. In [18-19], a control strategy is proposed based on the spatial repetitive controller (SRC) that utilizes the Lyapunov direct method to control the power consumption of the loads, maintaining the load voltage at the reference value. A switching pattern is proposed in [20] that is based on the space vector pulse width modulation (SVPWM) and controls a single stage current source boost inverter in order to achieve a desired frequency and voltage magnitude for both the islanded and grid-connected modes. In [21], a combinatorial droop control technique is proposed that utilizes a derivative controller in the islanded mode and an integral controller in the grid-connected mode to maintain the microgrid desired operation; the small-signal stability of the controller is also investigated for both scenarios. In [22], a control technique is proposed based on the direct-voltage control and optimized dynamic power sharing to eliminate the disturbances and minimize the switching actions in transition operating condition; it is demonstrated that this technique enhances the performance of the active damping controller and improves the dynamic response of the system. The integration of distributed battery energy storages into a local microgrid system is discussed in [23] and [24]. In [25], a microgrid consisting of a hybrid combination of inertial and converter interfaced DG units along with a nonlinear and unbalanced load is considered; it is demonstrated that it is possible to improve the power quality for such a system by allocating a DG unit as a power quality compensator for the load. In [26], a feed-forward current control technique is proposed for a microgrid converter that allows the interfaced converter to change its injected active and reactive power in the grid-connected mode by changing the voltage component and frequency. Several other control algorithms have been proposed to address different challenges associated the microgrids operation [27-29].

In this paper, a new control technique is proposed based on the Direct Lyapunov Control Method (DLCM) to determine the stable operating region of DG units in a microgrid. The impact of the instantaneous variations of the reference current components in the *ac*-side of the converters is carefully considered; also, the *dc*-voltage variations in the *dc*-side of the interfaced converters are discussed and properly addressed. Including these two problems in the proposed method is the main contribution of this work compared to the other existing control techniques.

The rest of the paper is organized into four sections. Following the introduction, general schematic diagram of the proposed microgrid system is introduced in Section III and its dynamic and state-space analysis are explained. Application of DLCM for the control and stable operation of DG units in different operating conditions is presented in Section IV. Moreover, simulation studies are carried out to demonstrate the efficiency and applicability of the developed control strategy in Section V. Finally, conclusion is provided in Section VI.

III. Description of the Proposed Model

Figure 1 illustrates the single-line diagram of the proposed microgrid model that can operate in both the grid-connected and islanded modes. The first unit (DG1) is set to inject the required active and reactive power of the local loads and then support the utility grid by injecting some extra power to the main grid. The second unit (DG2) is installed to be directly connected to the grid via the point of common coupling (PCC) in order to support the grid and supply the active and reactive power of the loads connected directly to the grid. The input power of DG units is provided by the local wind turbines. DG units can switch from the grid-connected mode to the islanded mode and vice versa using the corresponding switches in the proposed microgrid model. In addition, LC filters are used in the active and reactive power control loops to properly adjust the magnitude and frequency of the output voltage for each DG unit.

Figure 1

A. Mechanical Influences of Wind Turbine Systems in the proposed microgrid

The mechanical variables that contribute to generate *dc*-link voltage for DG units are analysed in this subsection. As it can be seen from Fig. 2, the power generation process of a wind turbine system is consisted of two parts, as mechanical and electrical [30]. According to this figure, three stages are employed to extract and regulate the wind power for loads and grid. The total mechanical power transformed by a wind turbine is expressed as,

$$P_{mech} = \frac{1}{2}\rho C_p A U_w^3 W \tag{1}$$

On the other hand, the curve of the power coefficient versus tip seed ratio with different values of β is used for various wind turbine applications [31]. The tip speed ratio is defined as,

$$\lambda = \frac{r\omega_m}{U_w} \tag{2}$$

The electromagnetic (EM) torque in the permanent magnet synchronous generator (PMSG) rotor is given as,

$$T_e = \left(\frac{3}{2}\right)\left(\frac{p}{2}\right)\left[\left(L_{dm} - L_{qm}\right) i_{qm} i_{dm} - \lambda_m i_{qm}\right] \tag{3}$$

Assuming $\omega_r = \frac{p}{2}\omega_m$, dynamic model of the PMSG can be expressed as,

$$\begin{aligned} v_{qm} &= -\left(R_m + L_{qm}\frac{d}{dt}\right) i_{qm} - \omega_r L_{dm} i_{dm} + \omega_r \lambda_m \\ v_{dm} &= -\left(R_m + L_{dm}\frac{d}{dt}\right) i_{dm} + \omega_r L_{qm} i_{qm} \end{aligned} \tag{4}$$

Where, the q-axis voltage is aligned with the terminal voltage of stator ($v_d = 0$). The power electronic converters are used for the appropriate control of PMSG in the second stage. In the third stage, the output voltages adaptation of PMSG is performed to reach the suitable *dc* or *ac* currents/voltages for the loads and/or grid. In real system, the speed of wind is variable; therefore, the output voltages and frequency of PMSG are variable. Equations (1)-(4) show that the variables ρ, C_p, A, U_w, W, r, and ω_m have negative impacts on the output voltages of PMSG in (4). Consequently, *dc*-link voltage will be an unbalanced. To deal with this challenge, a controller will be introduced in Section IV.

Figure 2

B. Dynamic model of the proposed microgrid scheme

The three phase configuration of the proposed microgrid model is depicted in Fig. 3. Each DG unit uses a three-phase voltage source inverter (VSI) as the interfacing system between the DG source, the loads, and/or the utility grid. Dynamic interactions between the current and voltage components of the proposed model should be properly modelled in order to design a proper control loop; the objectives are to achieve a proper power sharing between DG units, loads and/or grid, and current control of the DG units, and voltage control of the utility grid. According to Fig. 3, the dynamic model of the proposed microgrid system can be expressed as,

$$\begin{aligned} &L_{ci}\frac{di_{cki}}{dt} + R_{ci} i_{cki} - \left(S_{ki} - \frac{1}{3}\sum_{j=a}^{b.c} S_{ji}\right) v_{dci} + v_{ki} = 0 \\ &C_{fi}\frac{dv_k}{dt} = i_{fki} \\ &C_{dci}\frac{dv_{dc}}{dt} + \left(S_{ai} i_{cai} + S_{bi} i_{cbi} + S_{ci} i_{cci}\right) - i_{dci} = 0 \end{aligned} \tag{5}$$

The equivalent switching functions of the interfaced converters can be defined as,

$$u_{eqki} = -\left(S_{ki} - \frac{1}{3}\sum_{j=a}^{b.c} S_{ji} \right) \tag{6}$$

By substituting (6) into (5) and using the Park's transformation system, the dynamic model of the proposed control method can be achieved in the dq reference frame as,

$$\begin{aligned}
&L_{ci}\frac{di_{cdi}}{dt} + R_{ci}i_{cdi} - \omega L_{ci}i_{cqi} + u_{eq_{di}}v_{dci} + v_{di} = 0\\
&L_{ci}\frac{di_{cqi}}{dt} + R_{ci}i_{cqi} + \omega L_{ci}i_{cdi} + u_{eq_{qi}}v_{dci} + v_{qi} = 0\\
&C_{fi}\frac{dv_{di}}{dt} - \omega C_{fi}v_{qi} - i_{fdi} = 0\\
&C_{fi}\frac{dv_{qi}}{dt} + \omega C_{fi}v_{di} - i_{fqi} = 0\\
&C_{dci}\frac{dv_{dci}}{dt} - u_{eq_{di}}i_{cdi} - u_{eq_{qi}}i_{cqi} - i_{dci} = 0
\end{aligned} \tag{7}$$

Figure 3

C. Active and reactive power analysis of DG units

Defining the proper relation between the active and reactive power of the DG units allows the proposed control method to determine a suitable set-point for each interfaced VSI. According to (7), the steady-state model of the proposed microgrid system can be expressed as,

$$L_{ci}\frac{di^*_{cdi}}{dt} + R_{ci}i^*_{cdi} - \omega L_{ci}i^*_{cqi} + u^*_{eq_{di}}v^*_{dci} + v_{mi} = 0 \tag{8}$$

$$L_{ci}\frac{di^*_{cqi}}{dt} + R_{ci}i^*_{cqi} + \omega L_{ci}i^*_{cdi} + u^*_{eq_{qi}}v^*_{dci} = 0 \tag{9}$$

$$i^*_{fdi} = 0 \tag{10}$$

$$\omega C_{fi}v_{mi} - i^*_{fqi} = 0 \tag{11}$$

$$u^*_{eq_{di}}i^*_{cdi} + u^*_{eq_{di}}i^*_{cqi} + i^*_{dci} = 0 \tag{12}$$

Equations (10) and (11) verify that the filter capacitor (C_{fi}) generates the required reactive power to achieve the desired voltage amplitudes at the PCC during the steady-state operation, and it does not contribute to the active power generation ($i^*_{fdi} = 0,\ i^*_{fqi} = \omega C_{fi}v_{mi}$). Based on (8) and (9), the switching state functions of the interfaced VSI in the steady-state operating condition can be defined as,

$$u^*_{eq_{di}} = \frac{-L_{ci}I^*_{avdi} - R_{ci}i^*_{cdi} + \omega L_{ci}i^*_{cqi} - v_{mi}}{v^*_{dci}} \tag{13}$$

$$u^*_{eq_{qi}} = \frac{-L_{ci}I^*_{avqi} - R_{ci}i^*_{cqi} - \omega L_{ci}i^*_{cdi}}{v^*_{dci}} \tag{14}$$

where $I^*_{avji} = \dfrac{di^*_{cji}}{dt}$ expresses the average values of the instantaneous variations in the reference current components of the control loops for each DG unit during the steady-state operation; these variations are caused by the harmonic parts of the reference current components. By substituting (13) and (14) into (12), (15) can be obtained as,

$$\left[R_{ci}i^{*2}_{cdi} + \left(L_{ci}I^*_{avdi} + v_{mi}\right)i^*_{cdi}\right] + \left[R_{ci}i^{*2}_{cqi} + L_{ci}I^*_{avqi}i^*_{cqi}\right] - i^*_{dci}v^*_{dci} = 0 \tag{15}$$

Equation (15) can be rewritten as,

$$\left(i^*_{cdi} + \frac{L_{ci}I^*_{avdi} + v_{mi}}{2R_{ci}}\right)^2 + \left(i^*_{cqi} + \frac{L_{ci}I^*_{avqi}}{2R_{ci}}\right)^2 = \frac{\left(L_{ci}I^*_{avdi} + v_{mi}\right)^2 + \left(L_{ci}I^*_{avqi}\right)^2 + 4R_{ci}i^*_{dci}v^*_{dci}}{4R^2_{ci}} \tag{16}$$

Equation (16) determines the regions where the current components are injected or absorbed in the proposed microgrid model. During the steady-state operating condition, the active and reactive power of DG units are equal to $P^*_{DGi} = v_{mi}i^*_{cdi}$ and $Q^*_{DGi} = -v_{mi}i^*_{cqi}$; therefore, the acceptable region of active and reactive power for the DG units can be expressed as,

$$\left(P^*_{DGi} + \frac{L_{ci}I^*_{avdi}v_{mi} + v^2_{mi}}{2R_{ci}}\right)^2 + \left(Q^*_{DGi} - \frac{L_{ci}I^*_{avqi}v_{mi}}{2R_{ci}}\right)^2 = \frac{\left(L_{ci}I^*_{avdi}v_{mi} + v^2_{mi}\right)^2 + \left(L_{ci}I^*_{avqi}v_{mi}\right)^2 + 4R_{ci}i^*_{dci}v^*_{dci}v^2_{mi}}{4R^2_{ci}} \tag{17}$$

Equation (17) is in the general form of a circle expression, which is depicted in Fig. 4. This figure is referred to as the Capacity Curve (CC) of DG units under the steady-state operating condition, and demonstrates the maximum power injection capacity of each DG unit. The typical levels of active and reactive power generation for the DG units are shown in Fig. 4. As can be seen, the operating point of $\left(P^*_{DGi1}\ ,\ Q^*_{DGi1}\right)$ can be changed through the power vector in the steady-state condition as,

$$\sqrt{P^{*2}_{DGi} + Q^{*2}_{DGi}}\,.e^{jtng^{-1}\left(\frac{Q^*_{DGi}}{P^*_{DGi}}\right)} \tag{18}$$

According to the Equation (18), the new active and reactive power can be obtained based on the CC of each DG unit through the modification of the amplitude related to $\sqrt{P^{*2}_{DGi} + Q^{*2}_{DGi}}$ and the angle related to $tng^{-1}\left(\dfrac{Q^*_{DGi}}{P^*_{DGi}}\right)$.

Figure 4

D. Frequency and voltage variation analysis

Frequency and voltage regulation can be achieved through the proper sharing of the active and reactive power of each DG unit, both in dynamic and steady-state operating conditions. The variations of the DG current components and the dc-link voltage oscillations can be expressed in the dq frame as,

$$\frac{di_{cdi}}{dt}=\tilde{i}_{cdi},\ \frac{di_{cqi}}{dt}=\tilde{i}_{cqi},\ and\ \frac{dv_{dci}}{dt}=\tilde{v}_{dci} \tag{19}$$

The switching state function values of the interfaced converters in the connected DG units, $u_{eq_{di}}$ and $u_{eq_{qi}}$, can be calculated from the two first terms of (7); substituting those values into the last term of (7), the expression for the $i_{cdi}-i_{cqi}$ curve of each DG unit can be obtained as,

$$\left(i_{cdi}+\frac{L_{ci}\tilde{i}_{cdi}+v_{di}}{2R_{ci}}\right)^2+\left(i_{cqi}+\frac{L_{ci}\tilde{i}_{cqi}}{2R_{ci}}\right)^2=\frac{\left(L_{ci}\tilde{i}_{cdi}+v_{di}\right)^2+\left(L_{ci}\tilde{i}_{cqi}\right)^2+4R_{ci}\left(i_{dci}-C_{dci}\tilde{v}_{dci}\right)v_{dci}}{4R_{ci}^2} \tag{20}$$

The active and reactive power of each DG unit is equal to $P_{DGi}=v_{di}i_{cdi}$ and $Q_{DGi}=-v_{di}i_{cqi}$; hence, Equation (21) can be obtained as,

$$\left(P_{DGi}+\frac{L_{ci}\tilde{i}_{cdi}v_{di}+v_{di}^2}{2R_{ci}}\right)^2+\left(Q_{DGi}-\frac{L_{ci}\tilde{i}_{cqi}v_{di}}{2R_{ci}}\right)^2=\frac{\left(L_{ci}\tilde{i}_{cdi}v_{di}+v_{di}^2\right)^2+\left(L_{ci}\tilde{i}_{cqi}v_{di}\right)^2+4R_{ci}\left(i_{dci}-C_{dci}\tilde{v}_{dci}\right)v_{dci}v_{di}^2}{4R_{ci}^2} \tag{21}$$

where (21) is the equation of a circle with the centre of "c_i" $\left(=-\frac{L_{ci}\tilde{i}_{cdi}v_{di}+v_{di}^2}{2R_{ci}},\frac{L_{ci}\tilde{i}_{cqi}v_{di}}{2R_{ci}}\right)$ and the radius of "r_i" $\left(=\sqrt{\frac{\left(L_{ci}\tilde{i}_{cdi}v_{di}+v_{di}^2\right)^2+\left(L_{ci}\tilde{i}_{cqi}v_{di}\right)^2+4R_{ci}\left(i_{dci}-C_{dci}\tilde{v}_{dci}\right)v_{dci}v_{di}^2}{4R_{ci}^2}}\right)$.

According to (21), CC depends on the DG parameters, the variables R_{ci}, L_{ci} and C_{dci}, the output current and voltage components of DG units, the instantaneous variations of the reference current components, and the *dc*-side voltage. The centre and radius of CC can be changed by modifying the values of these variables and parameters.

The CC, P-f, and Q-E droop control characteristics of each DG unit are depicted in Fig. 5. The initial condition of DG units in the proposed microgrid model with the specific operating point 1 (op1) is depicted as CC1 in Fig. 5. As illustrated in this figure, with an increase in the values of the dispatched active and reactive power for each DG unit, the operating point will shift to op2. In addition, DG units track the reference frequency and voltage amplitude during the change in the power according to the droop control characteristics. CC3 indicates the operation of DG units during the islanded mode; during this operation mode, DG units inject active power to the load instead of the utility grid and consume reactive power ($Q_{DGi}<0$) in order to stabilize the voltage amplitude at the PCC. In this mode, the capacity curve of the DG unit (CC3) is around the op3.

As it can be seen from the P-f curve in Fig. 5, the active power increase in a DG unit decreases the frequency in the islanded mode; note that the frequency should be maintained within an acceptable range, e.g. $\pm 0.2 < \Delta f < \pm 0.4$. Furthermore, the Q-E curve demonstrates that increasing the value of negative reactive power in a DG unit increases the voltage magnitude.

Figure 5

Based on Eq. (21) and the capacity curves depicted in Fig. 5, the maximum active and reactive power of DG units can be obtained as,

$$P_{DGi\max} = \sqrt{\frac{\left(L_{ci}\tilde{i}_{cdi}v_{di} + v_{di}^2\right)^2 + \left(L_{ci}\tilde{i}_{cqi}v_{di}\right)^2 + 4R_{ci}\left(i_{dci} - C_{dci}\tilde{v}_{dci}\right)v_{dci}v_{di}^2}{4R_{ci}^2}} - \left|\frac{L_{ci}\tilde{i}_{cdi}v_{di} + v_{di}^2}{2R_{ci}}\right|$$
$$Q_{DGi\max} = \sqrt{\frac{\left(L_{ci}\tilde{i}_{cdi}v_{di} + v_{di}^2\right)^2 + \left(L_{ci}\tilde{i}_{cqi}v_{di}\right)^2 + 4R_{ci}\left(i_{dci} - C_{dci}\tilde{v}_{dci}\right)v_{dci}v_{di}^2}{4R_{ci}^2}} + \left|\frac{L_{ci}\tilde{i}_{cqi}v_{di}}{2R_{ci}}\right| \quad (22)$$

The active and reactive power of DG units during dynamic and steady state operating conditions can be expressed as,

$$P_{DGi}^* = P_{DGi} - \Delta P_{DGi}$$
$$Q_{DGi}^* = Q_{DGi} - \Delta Q_{DGi} \quad (23)$$

On the other hand, the equations of the droop control characteristics can be expressed as,

$$P_{DGi} = \frac{f_i^* - f_i}{m} \quad with \quad m = \frac{f_{\max i} - f_{\min i}}{P_{\max i}}$$
$$Q_{DGi} = \frac{E_i^* - E_i}{n} \quad with \quad n = \frac{E_{\max i} - E_{\min i}}{Q_{\max i}} \quad (24)$$

With respect to (24), (23) can be rewritten as,

$$P_{DGi}^* = \frac{f_i^* + \Delta f_i - f_i}{m}$$
$$Q_{DGi}^* = \frac{E_i^* + \Delta E_i - E_i}{n} \quad (25)$$

By substituting (25) into (17), (26) can be expressed as,

$$\left(\frac{f_i^* + \Delta f_i - f_i}{m} + \frac{L_{ci}I_{avdi}^* v_{mi} + v_{mi}^2}{2R_{ci}}\right)^2 + \left(\frac{E_i^* + \Delta E_i - E_i}{n} - \frac{L_{ci}I_{avqi}^* v_{mi}}{2R_{ci}}\right)^2 =$$
$$\frac{\left(L_{ci}I_{avdi}^* v_{mi} + v_{mi}^2\right)^2 + \left(L_{ci}I_{avqi}^* v_{mi}\right)^2 + 4R_{ci}i_{dci}^* v_{dci}^* v_{mi}^2}{4R_{ci}^2} \quad (26)$$

where (26) can be rewritten as,

$$\left(\frac{-1}{m} f_i + \frac{2R_{ci} f_i^* + 2R_{ci}\Delta f_i + mL_{ci} I_{avdi}^* v_{mi} + mv_{mi}^2}{2mR_{ci}}\right)^2 + \left(\frac{-1}{n} E_i + \frac{2R_{ci} E_i^* + 2R_{ci}\Delta E_i - nL_{ci} I_{avqi}^* v_{mi}}{2nR_{ci}}\right)^2 \quad (27)$$
$$= \frac{\left(L_{ci} I_{avdi}^* v_{mi} + v_{mi}^2\right)^2 + \left(L_{ci} I_{avqi}^* v_{mi}\right)^2 + 4R_{ci} i_{dci}^* v_{dci}^* v_{mi}^2}{4R_{ci}^2}$$

Therefore, the $E_i - f_i$ curve for each DG unit in the proposed microgrid model can be expressed as,

$$\frac{\left(f_i - \eta\right)^2}{m^2} + \frac{\left(E_i - \mu\right)^2}{n^2} = \varepsilon^2 \quad (28)$$

where,

$$\eta = \frac{2R_{ci} f_i^* + 2R_{ci}\Delta f_i + mL_{ci} I_{avdi}^* v_{mi} + mv_{mi}^2}{2R_{ci}}$$

$$\mu = \frac{2R_{ci} E_i^* + 2R_{ci}\Delta E_i - nL_{ci} I_{avqi}^* v_{mi}}{2R_{ci}}$$

$$\varepsilon = \sqrt{\frac{\left(L_{ci} I_{avdi}^* v_{mi} + v_{mi}^2\right)^2 + \left(L_{ci} I_{avqi}^* v_{mi}\right)^2 + 4R_{ci} i_{dci}^* v_{dci}^* v_{mi}^2}{4R_{ci}^2}}$$

Equation (28) is the equation of an ellipse with the centre of (η, μ) and the diameters of εm and εn respectively, as illustrated in Fig. 6.a.

This general curve is referred to as the $E-f$ control curve of the DG units in the proposed microgrid model. As it can be seen from the figure, the operating points on the $E-f$ control curves are dependent on the vector and angle amplitudes, with the values of "ℓ" ($=\sqrt{f_i^2 + E_i^2}$) and "∂" ($=\tan^{-1}\left(E_i / f_i\right)$). As it can be seen, the magnitude of the voltage vector increases when the frequency of the DG units decreases and vice versa. Figure 6.b depicts the different areas where the voltage magnitude and frequency are positive or negative. The regions with positive values for both E and f can be expanded by moving the centre of the ellipse toward the indicated arrow and increasing the ellipse's diameters. The $E-f$ control curves of the two different DG units are illustrated in Fig. 7. According to Fig. 7.a, as the centre of the $E-f$ control curve is changed, the DG2 unit cannot properly track the reference values of the voltage magnitude and frequency (f_i^*, E_i^*). In addition, according to Fig. 7.b, a decrease in the diameters of the $E-f$ control curve results in an inappropriate operation of DG2, as it cannot reach the desired values for the voltage magnitude and frequency.

Figures 6 and 7

IV. Proposed Control Technique

The Lyapunov control theory is utilized in this paper to analyse the dynamic behaviour of DG units and investigate the ability of the control loops to properly share the power in the proposed microgrid model. This control approach can ensure the global asymptotic stability for the DG units during the instantaneous variations of the reference current components, dc-side voltage oscillations, and any sudden changes in the parameters of the whole model. Next sections will describe the performance of the proposed Direct Lyapunov Control Method (DLCM) regarding the dynamic control in both the islanded and grid-connected modes.

A. Dynamic analysis of the proposed DLCM-based model

The two DG units in the proposed model are installed to support the utility grid by injecting active and reactive power and the harmonic current components of the nonlinear loads; this is done through the connection of the local power generation sources such as wind and solar and depends on the maximum capacity of the interfaced converter.

However, it should be considered that during the ideal situation the total injected power from the DG units should be sufficient for all the harmonics, required reactive power, and a portion of the loads active power consumption during the grid-connected mode, in a way that guarantees a unity power factor for the utility grid. In addition, the injected power from the DG units should be equal to the active and reactive power of the loads during the islanded mode. Based on the determined reference values of the current components, the grid voltage amplitude of the *ac*-side of the interfaced system, and the desired *dc*-voltage value in the *dc*-side of the interfaced converter, the errors in the proposed model can be achieved as,

$$x_{1i} = i_{cdi} - i_{cdi}^{*},\ \ x_{2i} = i_{cqi} - i_{cqi}^{*},\ \ x_{3i} = v_{di} - v_{di}^{*},\ \ x_{4i} = v_{qi} - v_{qi}^{*},\ \ x_{5i} = v_{dci} - v_{dci}^{*} \tag{29}$$

In addition, the switching functions dynamics of the interfaced converters can be defined as,

$$U_{eq_{di}} = u_{eq_{di}} - u_{eq_{di}}^{*} \tag{30}$$

$$U_{eq_{qi}} = u_{eq_{qi}} - u_{eq_{qi}}^{*} \tag{31}$$

According to equations (7) and (29)-(31), the dynamics of the error-based model of the closed-loop control method in the proposed microgrid can be obtained as,

$$\begin{aligned}
L_{ci}\frac{dx_{1i}}{dt} &= -R_{ci}x_{1i} + \omega L_{ci}x_{2i} - x_{3i} - u_{eq_{di}}x_{5i} - U_{eq_{di}}v_{dci}^{*} \\
L_{ci}\frac{dx_{2i}}{dt} &= -\omega L_{ci}x_{1i} - R_{ci}x_{2i} - x_{4i} - u_{eq_{qi}}x_{5i} - U_{eq_{qi}}v_{dci}^{*} \\
C_{fi}\frac{dx_{3i}}{dt} &= \omega C_{fi}x_{4i} + i_{fdi} - i_{fdi}^{*} \\
C_{fi}\frac{dx_{4i}}{dt} &= -\omega C_{fi}x_{3i} + i_{fqi} - i_{fqi}^{*} \\
C_{dci}\frac{dx_{5i}}{dt} &= u_{eq_{di}}x_{1i} + u_{eq_{qi}}x_{2i} + U_{eq_{di}}i_{di}^{*} + U_{eq_{qi}}i_{qi}^{*} + i_{dci} - i_{dci}^{*}
\end{aligned} \tag{32}$$

Based on DLCM theory, the proposed model is stable if the total level of the saved energy in the whole system is zero. By assuming $E(\bar{x})$ as the total level of the saved energy in the proposed model, the conditions listed below should be governed as,

$$\begin{aligned} &E(0)=0 \\ &E(\bar{x})>0 \ \forall \bar{x}\neq 0 \\ &E(\bar{x})\to\infty \ as \ \|\bar{x}\|\to\infty \\ &\dot{E}(\bar{x})<0 \ \forall \bar{x}\neq 0 \end{aligned} \tag{33}$$

With respect to (33), $E(\bar{x})$ is defined as,

$$E(x_{1i},x_{2i},x_{3i},x_{4i},x_{5i})=\frac{1}{2}L_{ci}x_{1i}^2+\frac{1}{2}L_{ci}x_{2i}^2+\frac{1}{2}C_{fi}x_{3i}^2+\frac{1}{2}C_{fi}x_{4i}^2+\frac{1}{2}C_{dci}x_{5i}^2 \tag{34}$$

The time derivative of (34) with respect to the error variables can be obtained as,

$$\dot{E}(x_{1i},x_{2i},x_{3i},x_{4i},x_{5i})=L_{ci}\dot{x}_{1i}x_{1i}+L_{ci}\dot{x}_{2i}x_{2i}+C_{fi}\dot{x}_{3i}x_{3i}+C_{fi}\dot{x}_{4i}x_{4i}+C_{dci}\dot{x}_{5i}x_{5i} \tag{35}$$

According to (32), (34) can be expressed as,

$$\begin{aligned} L_{ci}\dot{x}_{1i}x_{1i}&=-R_{ci}x_{1i}^2+\omega L_{ci}x_{2i}x_{1i}-x_{3i}x_{1i}-u_{eq_{di}}x_{5i}x_{1i}-U_{eq_{di}}v_{dci}^{*}x_{1i} \\ L_{ci}\dot{x}_{2i}x_{2i}&=-\omega L_{ci}x_{1i}x_{2i}-R_{ci}x_{2i}^2-x_{4i}x_{2i}-u_{eq_{qi}}x_{5i}x_{2i}-U_{eq_{qi}}v_{dci}^{*}x_{2i} \\ C_{fi}\dot{x}_{3i}x_{3i}&=\omega C_{fi}x_{4i}x_{3i}+\left(i_{fdi}-i_{fdi}^{*}\right)x_{3i} \\ C_{fi}\dot{x}_{4i}x_{4i}&=-\omega C_{fi}x_{3i}x_{4i}+\left(i_{fqi}-i_{fqi}^{*}\right)x_{4i} \\ C_{dci}\dot{x}_{5i}x_{5i}&=u_{eq_{di}}x_{1i}x_{5i}+u_{eq_{qi}}x_{2i}x_{5i}+U_{eq_{di}}i_{di}^{*}x_{5i}+U_{eq_{qi}}i_{qi}^{*}x_{5i}+\left(i_{dci}-i_{dci}^{*}\right)x_{5i} \end{aligned} \tag{36}$$

By substituting (36) into (35), the derivative of the total saved energy in the proposed microgrid model can be achieved as,

$$\begin{aligned} &\dot{E}(x_{1i},x_{2i},x_{3i},x_{4i},x_{5i})=-R_{ci}x_{1i}^2-R_{ci}x_{2i}^2-U_{eq_{di}}\left(v_{dci}^{*}x_{1i}-i_{di}^{*}x_{5i}\right)-U_{eq_{qi}}\left(v_{dci}^{*}x_{2i}-i_{qi}^{*}x_{5i}\right) \\ &\underline{-x_{3i}x_{1i}-x_{4i}x_{2i}+\left(i_{fdi}-i_{fdi}^{*}\right)x_{3i}+\left(i_{fqi}-i_{fqi}^{*}\right)x_{4i}+\left(i_{dci}-i_{dci}^{*}\right)x_{5i}} \end{aligned} \tag{37}$$

By assuming $\xi=\left(i_{fdi}-i_{fdi}^{*}\right)$ and $\kappa=\left(i_{fqi}-i_{fqi}^{*}\right)$, the underlined terms in (33) can be rewritten as,

$$\left(v_{di}-v_{di}^{*}\right)\left(\xi-x_{1i}\right)+\left(v_{qi}-v_{qi}^{*}\right)\left(\kappa-x_{2i}\right)+\left(v_{dci}-v_{dci}^{*}\right)\left(i_{dci}-i_{dci}^{*}\right) \tag{38}$$

As it can be seen from (38), given that the *dc*-link voltage is properly regulated around the set-point and the voltage amplitude at PCC is kept near the amplitude of the grid voltage, i.e., $v_{di}\to v_{di}^{*}$, $v_{qi}\to v_{qi}^{*}$ and $v_{dci}\to v_{dci}^{*}$, (37) satisfies the Lyapunov stability conditions if the steady-state values of the switching functions are considered as,

$$U_{eq_{di}}=\alpha_i\left(v_{dci}^{*}x_{1i}-i_{cdi}^{*}x_{5i}\right) \tag{39}$$

$$U_{eq_{qi}} = \beta_i \left(v^*_{dci} x_{2i} - i^*_{cqi} x_{5i} \right) \tag{40}$$

where α_i and β_i are the constant and positive coefficient values.

As it can be seen from (39) and (40), if the *d* and *q* current components of DG units and the dc-link voltage are deviated from their desired values, the switching functions dynamics of the interfaced converters will be activated, and subsequently, the VSI follows the reference current and voltage components with a fast dynamic response in order to compensate for the generated errors.

B. Calculation of reference current components in DG control loop

The accurate operation of DG units for the active and reactive power sharing in a microgrid system is highly dependent on the proper calculation of the reference values of the current components in the control loop of the DG units. Given that the output active and reactive power of the DG units are $P_{DGi} = v_{di} i_{cdi}$ and $Q_{DGi} = -v_{di} i_{cqi}$, the injected power from DG units can be independently controlled by regulating the DG currents. In the proposed microgrid model, it is expected that the reactive power of the local and main loads should be supplied by DG1 and DG2 respectively. Thus,

$$\begin{aligned} i_{cq1} &= i_{llq} \\ i_{cq2} &= i_{mlq} \end{aligned} \tag{41}$$

On the other hand, the harmonic components of the active power of the local and main loads should be compensated by DG1 and DG2 respectively. Also, the fundamental component of the total active power of the local load and a fraction of the active power of the main load will be generated by DG1. If we consider the d-component of the local and main loads as,

$$\begin{aligned} i_{lld} &= \tilde{i}_{lld} + I_{lld1} \\ i_{mld} &= \tilde{i}_{mld} + I_{mld1} \end{aligned} \tag{42}$$

then, the reference currents of the *d*-axis in the DG1 and DG2 units can be expressed as,

$$\begin{aligned} i_{cd1} &= \tilde{i}_{lld} + I_{lld1} + \chi I_{mld1} \\ i_{cd2} &= \tilde{i}_{mld} + \left(1 - \chi\right) I_{mld1} \end{aligned} \tag{43}$$

Figure 8 demonstrates the general block diagram for the reference current calculation of each DG unit in the proposed microgrid model. As it can be seen, a low pass filter (LPF) is utilized to extract the loads current harmonics in *d*-axis. Also, a proportional-integral (PI) linear controller is used to minimize the error between the injected currents from the DG units and reference currents values; not that the regulation of the PI gains can impact the dynamic and steady-state responses.

Figure 8

C. Stability analysis of dc-link voltage

By considering $u_{dci} = C_{dci} \dfrac{dv_{dci}}{dt}$ in the last term of (7), (44) can be given as [32],

$$u_{dci} = u_{eq_{di}} i_{cdi} + u_{eq_{qi}} i_{cqi} + i_{dci} \tag{44}$$

In order to regulate the dc-link voltage at a fixed value, the error $\Delta v_{dci} = v_{dci}^{*} - v_{dci}$ is passed through a PI-type compensator.

$$u_{dci} = k_{pi} \Delta v_{dci} + k_{Ii} \int \Delta v_{dci} dt \tag{45}$$

The closed loop control of dc-link voltage regulator is shown in Fig.9. The closed loop transfer function of *dc*-link voltage regulation can be achieved as,

$$G_i(s) = \frac{v_{dci}(s)}{v_{dci}^{*}(s)} = 2\zeta_i \omega_{xi} \frac{s + \frac{\omega_{xi}}{2\zeta_i}}{s^2 + 2\zeta_i \omega_{xi} s + \omega_{xi}^2}, \quad k_{pi} = 2\zeta_i \omega_{xi} C_{dci}, \quad k_{Ii} = \omega_{xi}^2 C_{dci} \tag{46}$$

Where ω_{xi} is natural un-damped angular frequency and depends on the specific time response.

According to (44), i_{cdi} can be achieved as,

$$i_{cdi} = \frac{u_{dci} - u_{eq_{qi}} i_{cqi} - i_{dci}}{u_{eq_{di}}} = \frac{u_{dci} v_{dci} - u_{eq_{qi}} i_{cqi} v_{dci} - i_{dci} v_{dci}}{u_{eq_{di}} v_{dci}} \tag{47}$$

Figure 9

On the other hand, assuming the supply voltages are given by,

$$\begin{aligned} v_a &= v_m \cos(\omega t) \\ v_b &= v_m \cos\left(\omega t - \frac{2\pi}{3}\right) \\ v_c &= v_m \cos\left(\omega t - \frac{4\pi}{3}\right) \end{aligned} \tag{48}$$

The transformation to the synchronous reference frame yields,

$$\begin{bmatrix} V_d \\ V_q \end{bmatrix} = \sqrt{2} \begin{bmatrix} \cos\left(\theta - \frac{\pi}{6}\right) & \sin(\theta) \\ -\sin\left(\theta - \frac{\pi}{6}\right) & \cos(\theta) \end{bmatrix} \begin{bmatrix} v_a \\ v_b \end{bmatrix} \tag{49}$$

as a result,

$$u_{eq_{qi}} v_{dci} \cong V_q = 0, \quad u_{eq_{di}} v_{dci} \cong V_d = \sqrt{\frac{3}{2}} v_m \tag{50}$$

The control effort can be approximated as,

$$i_{h1_{di}}^{*} \cong \sqrt{\frac{2}{3}} \frac{u_{dci} v_{dci} - i_{dci} v_{dci}}{v_m} \tag{51}$$

The reference current in (51) is added to the reference current of the control loop of i_{ld} to guarantee a zero error value for *dc*-link voltage of each DG unit.

V. Results and Discussions

The performance of the proposed control strategy in the microgrid model is evaluated in transient and steady-state operating conditions using the Matlab/Simulink "SimPowerSystems" toolbox. The general schematic diagram of the whole model including the grid, load, and control parts is illustrated in Fig. 10. All parameters of the proposed model are given in the Appendix.

Two three-phase diode rectifiers with the R-L loads of $10+j\pi\,\Omega$ and $40+j\pi\,\Omega$ are considered as the main and local nonlinear loads, respectively. Simulation sequences are based on the on/off modes of the switches as depicted in the single-line multi DGs microgrid model in Fig. 11. This assessment consists of three states:

Operating Mode 1: Main load is supplied by the utility grid and the local load is supplied by DG1 (S1=on, S2=S3=off, refer to Fig. 11.a). This state is referred to as isolated mode in which DG units are not connected to each other and operate separately and independently.

Operating Mode 2: Both the DG units are connected to the utility grid (S1=S2=S3=on, refer to Fig. 11.b).

Operating Mode 3: Loads are supplied by the DG units (S1=off, S2=S3=on, refer to Fig. 11.c). This state is referred to as islanded mode in which DG units are connected to each other.

Figures 10 and 11

A. Evaluation of process 1 (Operating Mode 1 to Operating Mode 2)

As illustrated in Fig. 11.a, the main and local loads are supplied by the utility grid and DG1, respectively. In order to compensate for the reactive power of the loads and the injection of the maximum active power from the DG units into the utility grid in the grid-connected mode, S2 and S3 are turned on at t=0.14 s, as depicted in Fig. 11.b.

Figures 12 to 14 demonstrate the active and reactive power sharing between the main and local loads, grid and DG units based on the loads power consumption; it also demonstrates the frequency and voltage variations of the grid and DG units during the transition of the proposed model from the isolated mode to the grid-connected mode at t= 0.14 s.

Figure 12 shows that prior to entering the grid-connected mode, the total active power of the main load is supplied by the utility grid; however, after the connection of DG units to the utility grid, the injected active power from the grid to the load decreases to 5kW due to the fast dynamic response of the proposed control technique. In addition, DG2 injects the maximum active power of the fundamental frequency; this power is determined by the reference active power in the current control loop of the DG units. DG2 also injects all the harmonic current components. As it can be seen, the total active power of the local load for both the main and harmonic frequencies are supplied by DG1; however, after the transition from the islanded mode to the grid-connected mode, DG1 supplies the total active power of the local load, and remained active power is injected to the main load. Consequently, the active power injected by the grid is significantly decreased.

Figure 12

Figure 13 shows the reactive power sharing between the main and the local loads, grid, and DG units during the transition of the microgrid model from the isolated mode to the grid-connected mode at t= 0.14 s. As it can be seen, DG2 provides the total reactive power of the main load. Such behaviour from DG2 indicates a unity power factor for the utility grid. In addition, when DG1 is in the isolated mode, the total reactive power generated by the filter capacitance C_{f1} is consumed by DG1 to create a balanced and sinusoidal voltage at the PCC. Furthermore, under the appropriate dynamic operation of the controller, DG1 generates the total reactive power of the local load both in the isolated and grid-connected modes.

Figure 13

Figure 14 illustrates the comparison between the frequencies of the utility grid and DG units and changes in the voltage magnitudes of each DG unit during the transition to the grid-connected mode. As it can be seen, there are some small oscillations in the frequency of DG units during the transition to the grid-connected operating mode; on the other hand, the voltage magnitudes of DG units successfully reach the grid voltage magnitude during a short transient time.

Figure 14

B. Evaluation of process 2 (Operating Mode 2 to Operating Mode 3)

The proposed microgrid model shifts from the grid-connected mode to the islanded mode at t=0.28 s; in the islanded operating mode, DG1 and DG2 should properly share their maximum active power between the local and the main loads.

Figures 15 and 16 show the active and reactive power sharing between the main and the local loads, grid, and DG units, respectively. As it can be seen from Fig. 15, after t=0.28 s, the active power of the utility grid becomes zero as DG2 starts to inject active power comprised with all the harmonic current components of the main load in the d-axis.

In order to reach the desired voltage magnitude at the PCC, DG2 consumes the reactive power generated by the filter capacitor C_{fi} as shown in Fig. 16.

Figures 15 and 16

As it can be seen in Fig. 15, during the islanded mode the active power of DG1 is abruptly increased to compensate for the active power of the grid. Furthermore, generated reactive power from the filter capacitor is absorbed by DG1 with a slow dynamic response to fix the voltage magnitude at the PCC, as depicted in Fig. 16. The variations in the frequency of DG units and the voltage amplitude at the PCC are illustrated in Fig. 17. As it can be seen from this figure, the frequency of the DG units reaches the grid frequency after the system fully transit to the islanded mode. In addition, the steady-state value of the voltage amplitude at the PCC is close to the amplitude of the grid voltage.

Figure 17

C. *Harmonic current compensation*

Figure 18 illustrates the main and local loads, DG units and utility grid currents in both the isolated and grid-connected modes. As it can be seen, both units completely compensate for the harmonic current components of the local and main loads, respectively. Therefore, the grid current is sinusoidal and in phase with the grid voltage. To evaluate the capabilities of the proposed control method to compensate for the harmonic current components of the nonlinear loads, the spectra of the grid and load currents are shown in Fig. 19 during the grid-connected mode. Figures 19(a) and 19(b) demonstrate that THD of the main and local loads are 19.1% and 18.9%, respectively. But, Fig. 19(c) shows that THD of the grid current reaches 1.4% after connection of the DG units into the grid, confirming the capabilities of the proposed control method to compensate for the harmonic current components of the nonlinear loads.

Figures 18 and 19

VI. Conclusion

A control technique was presented based on the Lyapunov theory for the stable operation of DG units during the grid-connected and islanded modes in a microgrid. As the main contribution, the proposed technique compensates for the instantaneous variations of the reference current components of DG units in the *ac*-side. The presented method also considers and properly addresses the *dc*-voltage variations in the *dc*-side of the interfacing system. Simulation results confirmed that by implementation of the proposed control technique, DG units can provide a continuous active power for the loads and the utility grid. Furthermore, the proposed control method has a fast dynamic response to provide the reactive power and harmonic current components of the nonlinear loads; the active power of the fundamental frequency will be supplied by the utility grid, and hence, the grid will have a unity power factor. The proposed control method can be used for the integration of different types of DG sources, especially those that are based on the renewable energy resources to supply the local loads. It can also be utilized to enhance the power quality in a custom power distribution grid. Future work can include the robust performance of the control technique in presence of variations in the system parameters and unbalanced grid voltages.

Acknowledgements

This work was supported by FEDER funds (European Union) through COMPETE, and by Portuguese funds through FCT, under Projects FCOMP-01-0124-FEDER-020282 (Ref. PTDC/EEA-EEL/118519/2010) and UID/CEC/50021/2013. Also, the research leading to these results received funding from the EU Seventh Framework Programme FP7/2007–2013 under grant agreement no. 309048.

Appendix

$\alpha = 0.01, \beta = 0.1, v_s = 380volt, v_{dci} = 1200volt, R_{ci} = 0.1\Omega, L_{ci} = 45mH, R_g = 0.1\Omega, L_g = 0.1mH, P_{DG1} = 6.5kW$

$P_{DG2} = 10kW, Q_{DG1} = 6kVA, Q_{DG2} = 8kVA, f_{si} = 10kHz$

References

[1] Akorede MF, Hizam H, Pouresmaeil E. Distributed energy resources and benefits to the environment. Renewable and Sustainable Energy Reviews 2010; 14(2): 724–734.

[2] Hartono B S, Budiyanto Y, Setiabudy R. Review of microgrid technology. International Conference on QiR (Quality in Research) 2013: 127 – 132.

[3] Zhang Z, Huang X, Jiang J, Wu B. A load-sharing control scheme for a microgrid with a fixed frequency inverter. Electric Power Systems Research 2010; 80(3): 311–317.

[4] Guerrero J M, Matas J, De Vicuna L G, Castilla M, Miret J. Decentralized control for parallel operation of distributed generation inverters using resistive output impedance. IEEE Trans Industrial Electron 2007; 54(2): 994–1004.

[5] Guerrero J M, Chandorkar M, Lee T-L, Loh P C. Advanced control architecture for intelligent microgrids-PartI: Decentralized and Hierarchical Control. IEEE Trans Industrial Electron 2013; 60(4): 1254–1262.

[6] Mehrizi-sani A, Iravani R. Potential-Function based control of a microgrid in islanded and grid-connected modes. IEEE Trans Power System 2010; 25(4): 1883–1891.

[7] Ahn S-J, Park J-W, Chung I-Y, Moon S-I, Kang S-H, Nam S-R. Power-sharing method of multiple distributed generators considering control modes and configurations of a microgrid. IEEE Trans Power Delivery 2010; 25(3): 2007–2016.

[8] Katiraei F, Iravani M R. Power management strategies for a microgrid with multiple distributed generation units. IEEE Trans Power Systems 2006; 21(4): 1821–1831.

[9] Chung I-Y, Liu W, Cartes D A, Collins Jr E G, Moon S-I. Control methods of inverter-interfaced distributed generators in a microgrid system. IEEE Trans Industrial Electron 2010; 46(3):1078–1088.

[10] Abusara M A, Guerrero J M, Sharkh S M. Line-Interactive UPS for Microgrids. IEEE Trans Industrial Elects 2014; 61(3): 1292-1300.

[11] Balaguer I J, Lei Q, Yang S, Supatti U, Peng F Z. Control for Grid-Connected and Intentional Islanding Operations of Distributed Power Generation. IEEE Trans Industrial Elects 2011; 58(1): 147-157.

[12] Lei Q, Peng F Z, Yang S. Multiloop Control Method for High-Performance Microgrid Inverter Through Load Voltage and Current Decoupling With Only Output Voltage Feedback. IEEE Trans Power Elects 2011; 26(3): 953-960.

[13] Ahn S J, Park J W, Chung I Y, Moon S I, Kang S H, Nam S R. Power-Sharing Method of Multiple Distributed Generators Considering Control Modes and Configurations of a Microgrid. IEEE. Trans. Power Delivery 2010; 25 (3): 2007-2016.

[14] Li Y, Vilathgamuwa D M, Loh P C. Design, analysis, and real-time testing of a controller for multibus microgrid system. IEEE. Trans. Power Electron. 2004; 19(5): 1195–1204.

[15] Katiraei F, Iravani M R. Power management strategies for a microgrid with multiple distributed generation units. IEEE Trans. Power Syst. 2006; 21(4): 1821–1831.

[16] Li Y W, Kao C N. An Accurate Power Control Strategy for Power Electronics-Interfaced Distributed Generation Units Operating in a Low-Voltage Multibus Microgrid. IEEE Trans. Power Electron. 2009; 24(12): 2977–2988.
[17] Kim J, Lee J, Nam K. Inverter-Based Local AC Bus Voltage Control Utilizing Two DOF Control. IEEE Trans Power Electron 2008; 23(3): 1288–1298.
[18] Dasgupta S, Sahoo S K, Panda S K. Single-Phase Inverter-Control Techniques for Interfacing Renewable Energy Sources With Microgrid—Part I: Parallel-Connected Inverter Topology With Active and Reactive Power Flow Control Along With Grid Current Shaping. IEEE Trans Power Electron 2011; 26(3): 717–731.
[19] Dasgupta S, Mohan S N, Sahoo S K, Panda S K,. Lyapunov Function-Based Current Controller to Control Active and Reactive Power Flow From a Renewable Energy Source to a Generalized Three-Phase Microgrid System. IEEE Trans Industrial Electron 2013; 60(2): 799–813.
[20] Mirafzal B, Saghaleini M, Kaviani A K. An SVPWM-Based Switching Pattern for Stand-Alone and Grid-Connected Three-Phase Single-Stage Boost Inverters. IEEE Trans Power Electron 2011; 26(4): 1102–1111.
[21] Kim J, Guerrero J M, Rodriguez P, Teodorescu R, Nam K. Mode Adaptive Droop Control With Virtual Output Impedances for an Inverter-Based Flexible AC Microgrid. IEEE Trans Power Electron 2011; 26(3): 689–701.
[22] Mohamed Y A-R I, Zeineldin H, Salama M A, Seethapathy R. Seamless Formation and Robust Control of Distributed Generation Microgrids via Direct Voltage Control and Optimized Dynamic Power Sharing. IEEE Trans Power Electron 2012; 27(3): 1283–1294.
[23] Quesada J, Sebastian R, Castro M, Sainz J A. Control of inverters in a low voltage microgrid with distributed battery energy storage, Part I: Primary control. Electric Power Systems Research 2014; 114: 126–135.
[24] Cardoso G, Stadler M , Siddiqui A, Marnay C, DeForest N, Barbosa-Póvoa A, Ferrão P. Microgrid reliability modeling and battery scheduling using stochastic linear programming. Electric Power Systems Research 2013; 103: 61–69.
[25] Shahnia F, Majumder R, Ghosh A, Ledwich G, Zare F. Operation and control of a hybrid microgrid containing unbalanced and nonlinear loads. Electric Power Systems Research 2010; 80(8): 954–965.
[26] Arboleya P, Diaz D, Guerrero J M, Garcia P, Briz F, Gonzalez-Moran C, Aleixandre J G . An improved control scheme based in droop characteristic for microgrid converters. Electric Power Systems Research 2010; 80(10): 1215–1221.
[27] Dou C, Jia X, Bo Z, Liu D, Zhao F. Hybrid Control for Micro-Grid Based on Hybrid System Theory. Power and Energy Society General Meeting, 2011 IEEE: 1-10.
[28] Schiffer J, Ortega R, Astolfi A, Raisch J, Sezi T. Conditions for Stability of Droop-Controlled Inverter-Based Microgrids. Automatica 2014.
[29] Andrade F, Kampouropoulos K, Cusido J, Romeral L. Stability Analysis of a Microgrid System based on Inverter-Interfaced Distributed Generators. Advances in Electrical and Computer Engineering 2013; 13(3): 17–22.
[30] Teodorescu R, Liserre M, Rodriguez P. Grid Converters for Photovoltaic and Wind Power Systems. John Wiley & Sons 2011; 1–407.
[31] Tan K, Islam S. Optimum Control Strategies in Energy Conversion of PMSG Wind Turbine System without Mechanical Sensors. . IEEE Trans Energy Conversion 2004; 19(2): 392–399.
[32] Mehrasa M, Adabi M.E, Pouresmaeil E, Adabi J. Passivity based control technique for integration of DG resources into the power grid. Int. J. Elect. Power Energy System 2014; 58: 281–290.

Figure Captions

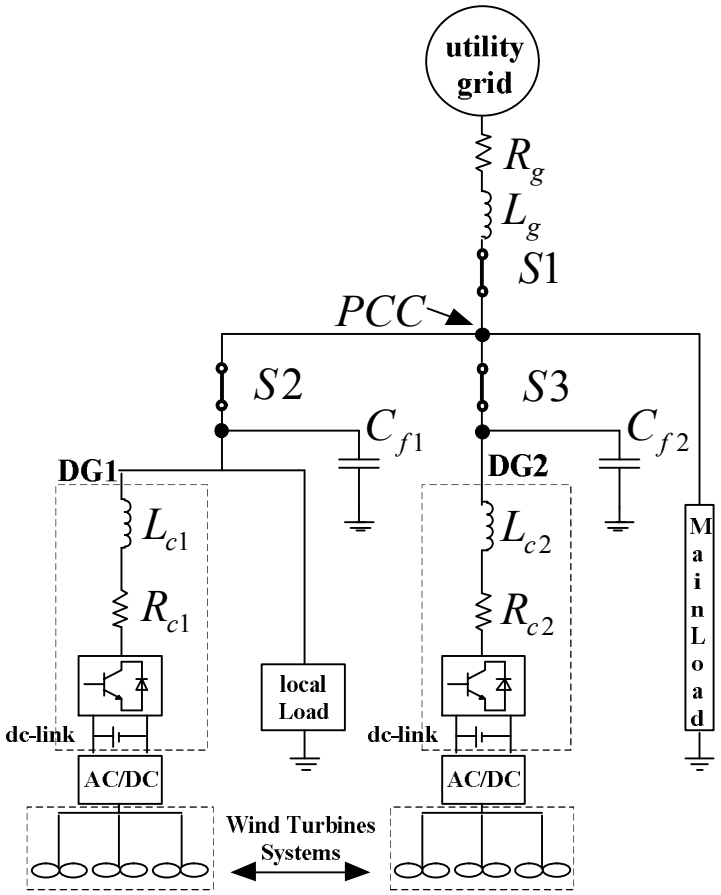

Fig. 1. Single-line diagram of the proposed Microgrid model.

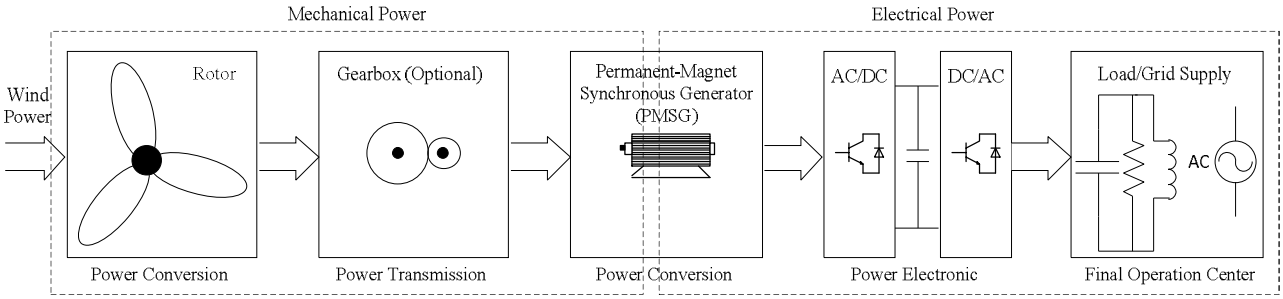

Fig. 2. Power conversion process of WTS.

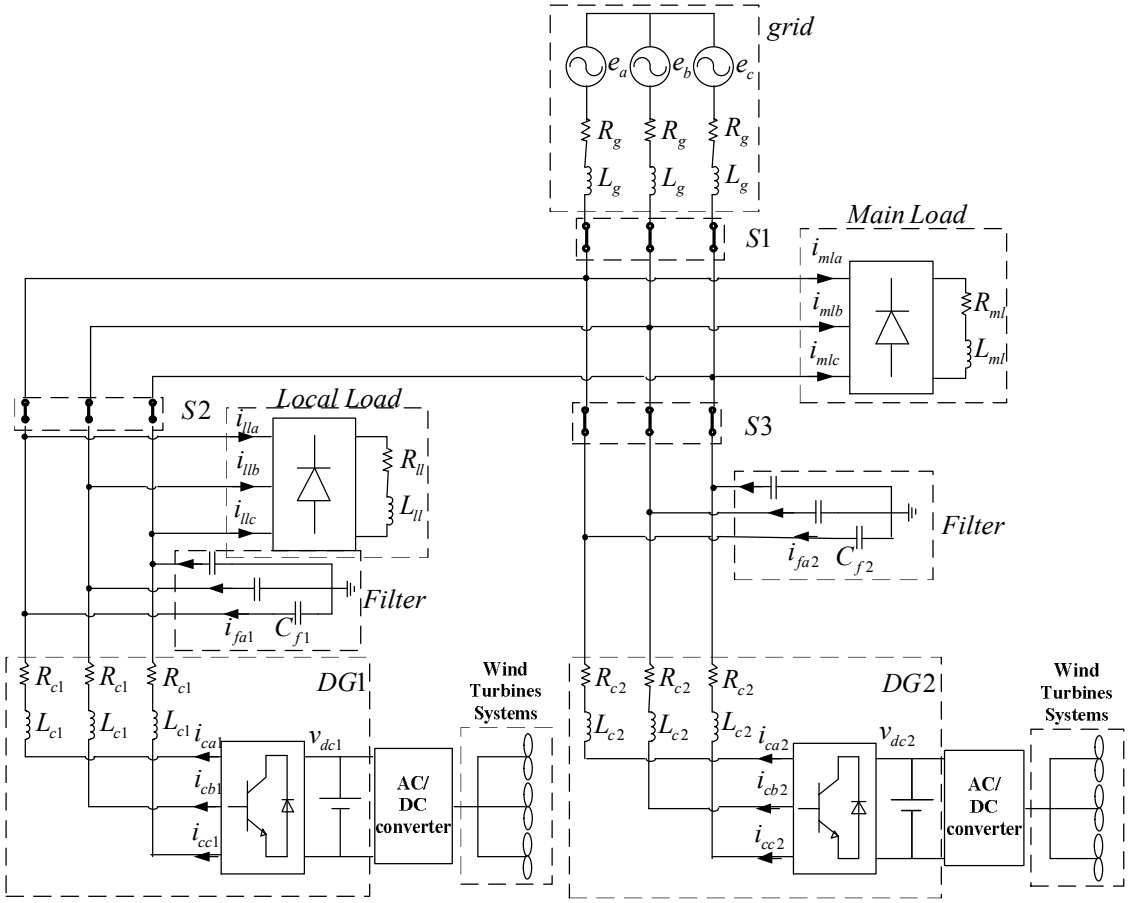

Fig. 3. General configuration of the proposed Microgrid model.

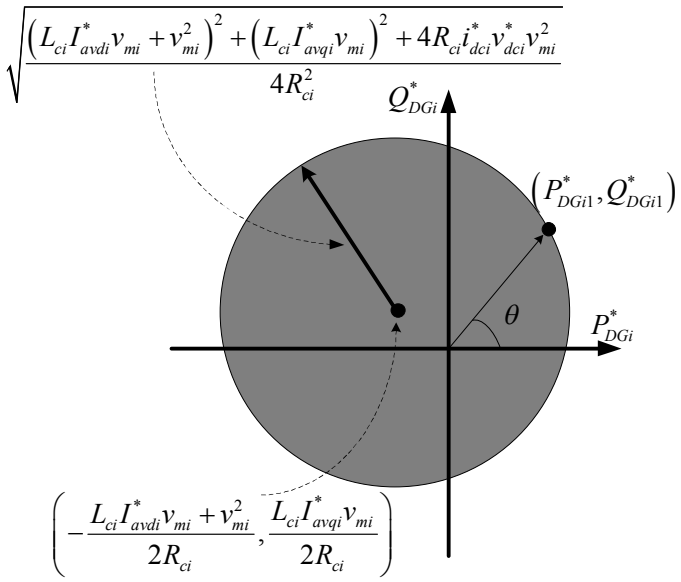

Fig. 4. Capacity Curve (CC) of DG units under the steady state operating condition.

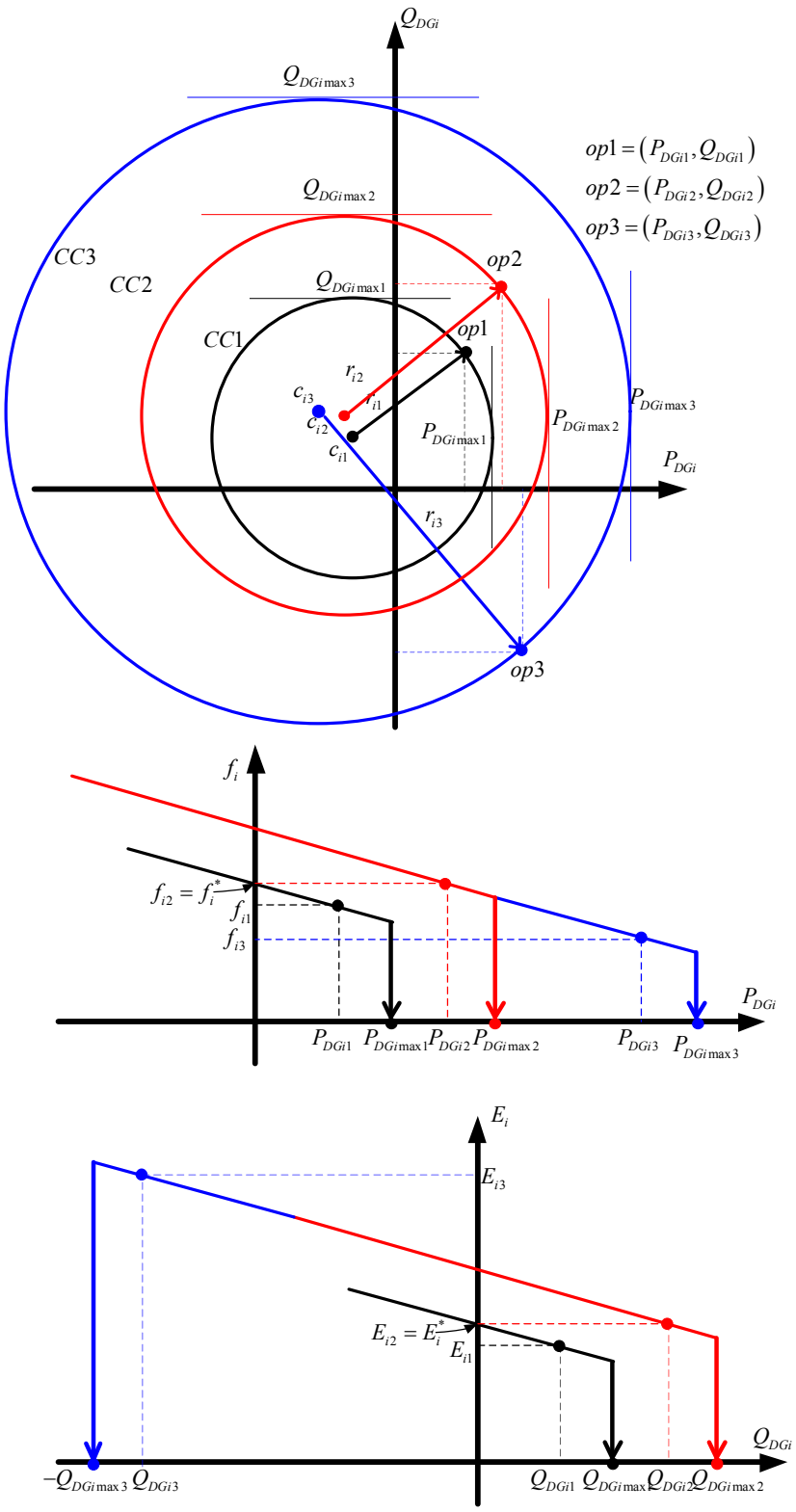

Fig. 5. Capacity curve, P-f, and Q-E droop control of DG units.

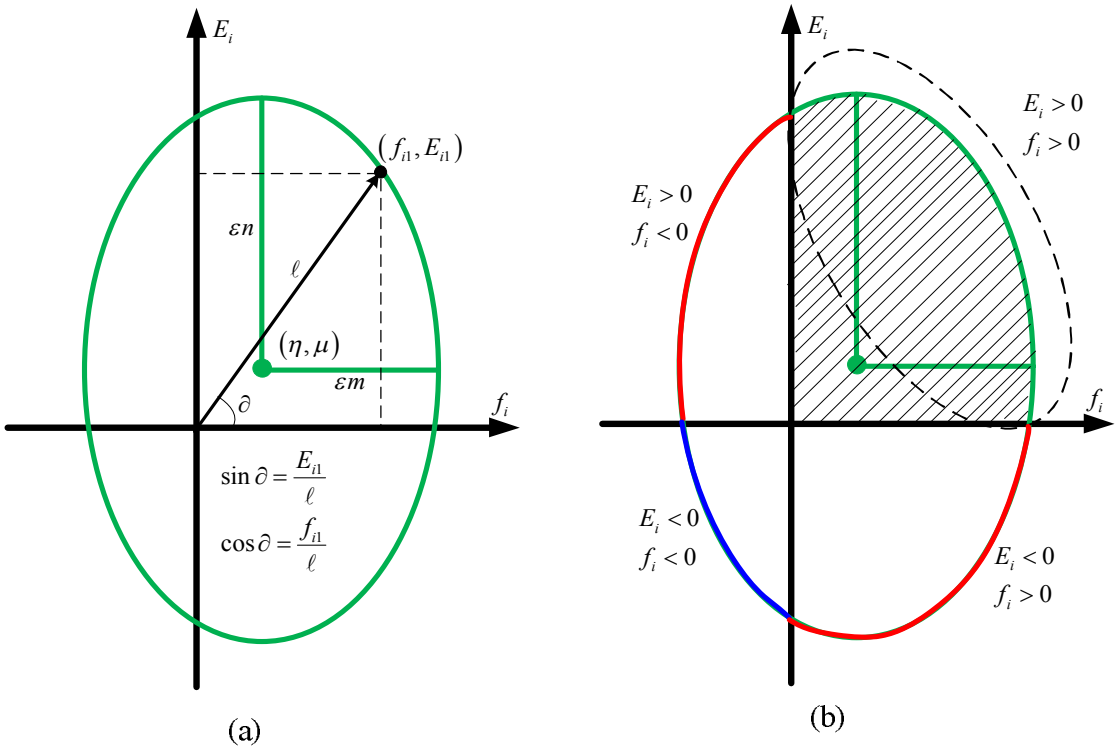

Fig. 6. The $E-f$ control curve of DG unit (a) different specification (b) positive or negative regions.

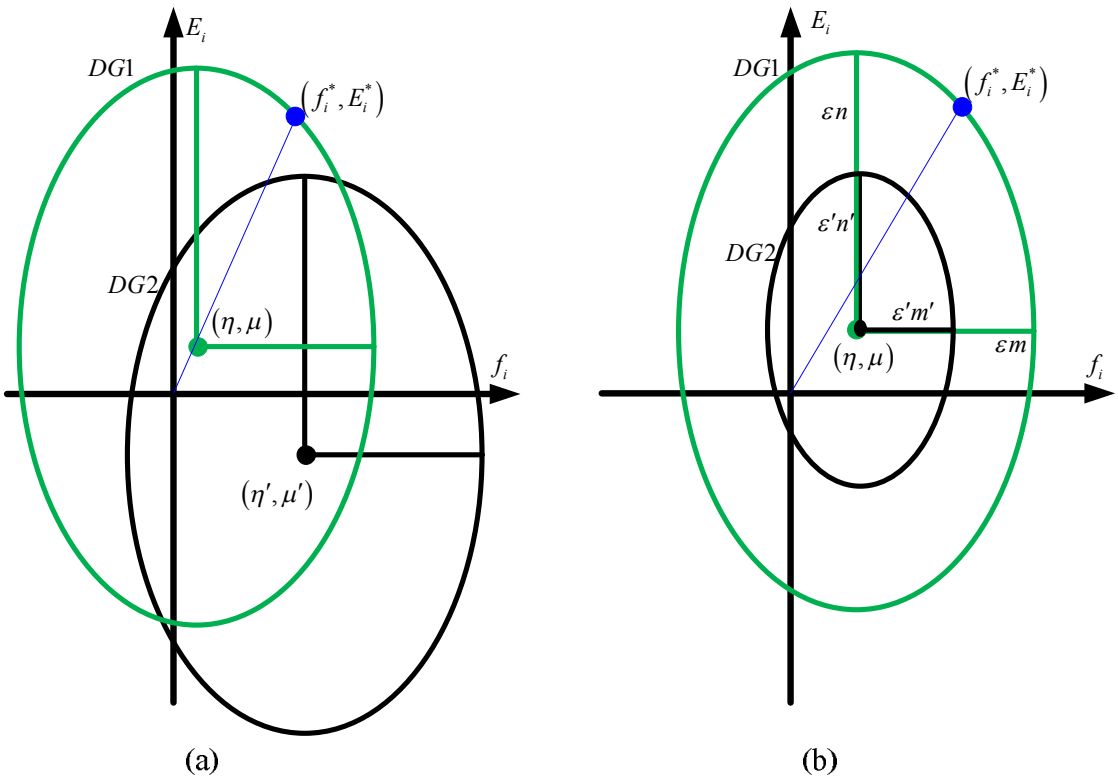

Fig. 7. The $E-f$ control curve of two different DG units (a) change in diameters (b) change in centers.

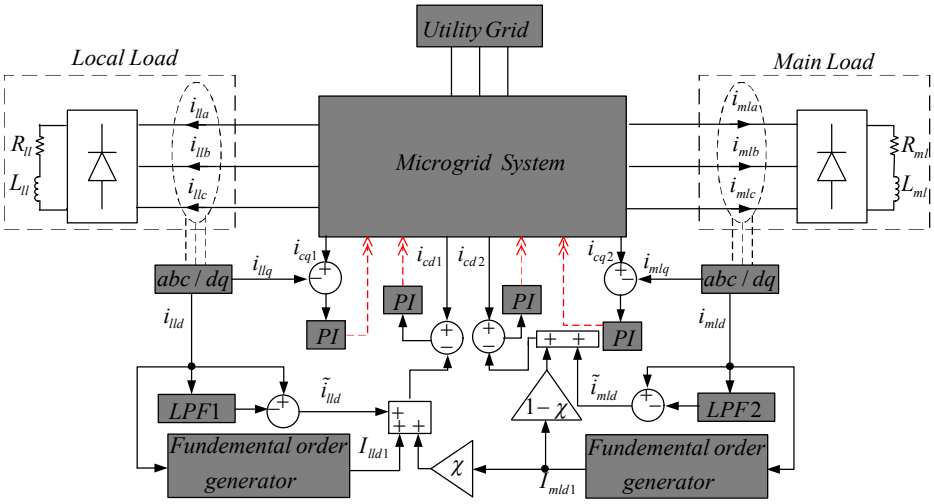

Fig. 8. Reference current calculation of DG units.

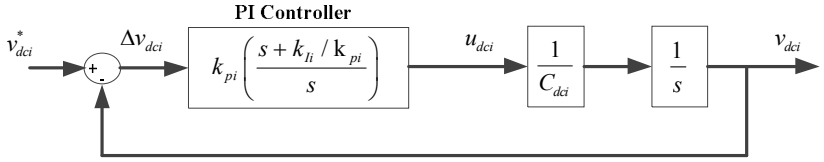

Fig. 9. Control loop of the input voltage.

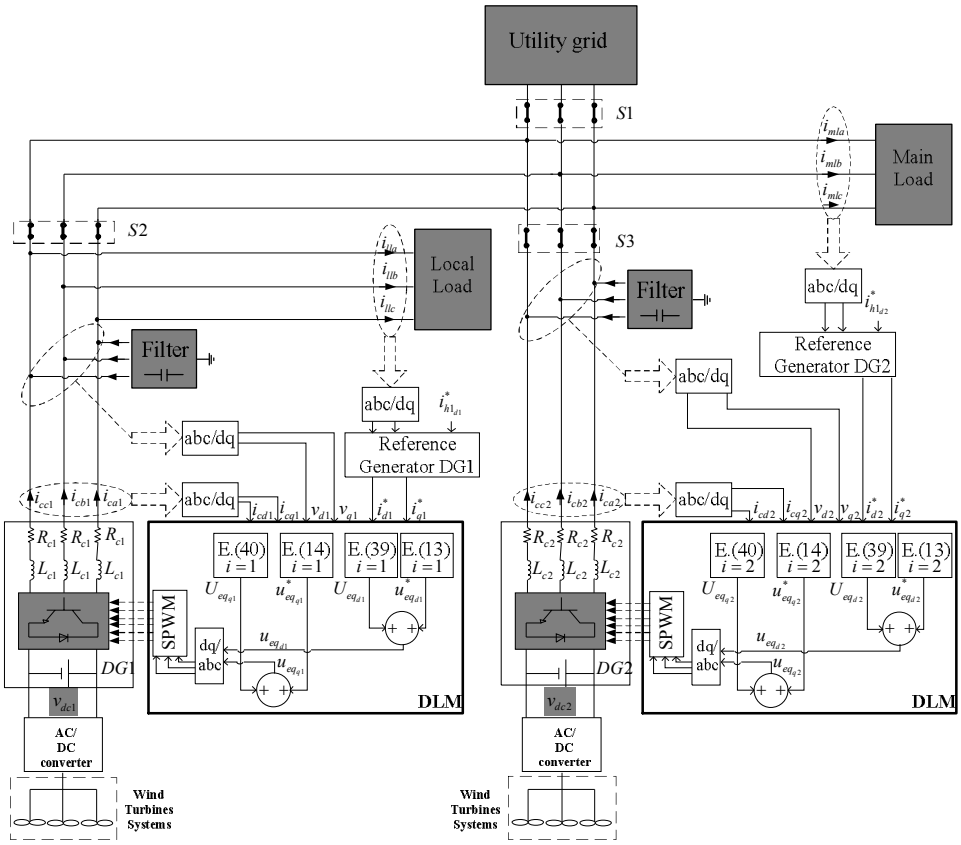

Fig. 10. General schematic diagram of the proposed model and control technique.

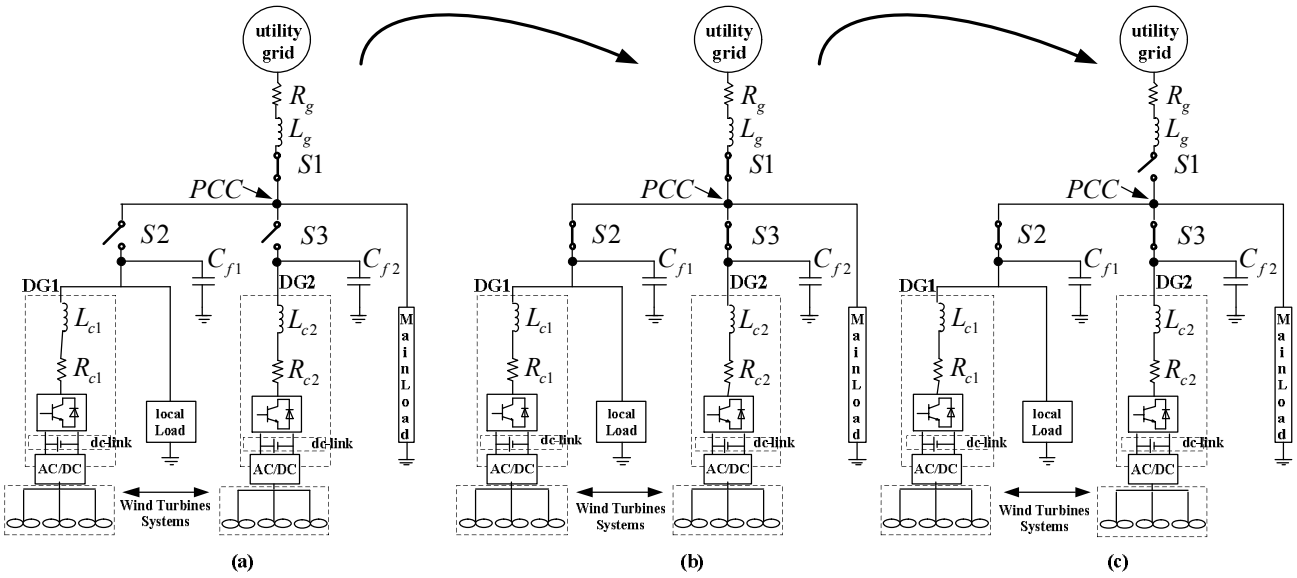

Fig. 11. Different operating modes of the proposed microgrid model a) isolated mode, b) grid-connected mode, and c) islanded mode.

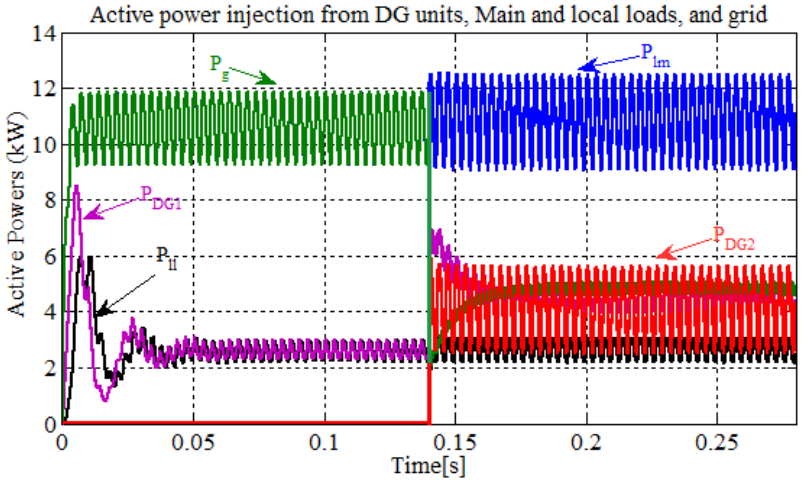

Fig. 12. The active power sharing between the main and local loads, grid and DG units during the conversion from isolated mode to the grid-connected mode.

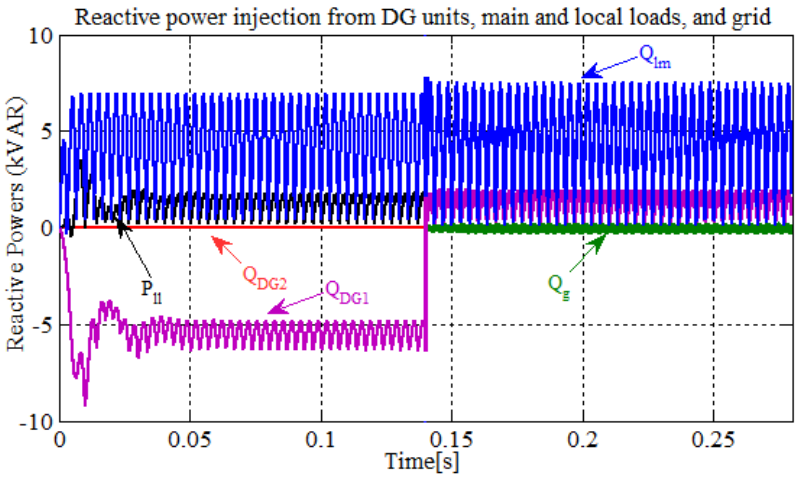

Fig. 13. The reactive power sharing between the main and local loads, grid, and DG units during the conversion from isolated mode to the grid-connected mode.

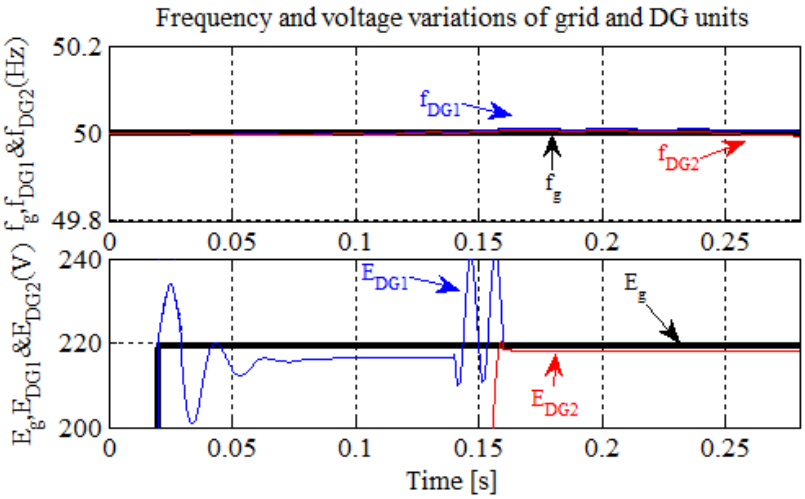

Fig. 14. The frequency and voltage variations in grid and DG units during the conversion from the isolated mode to the grid-connected mode.

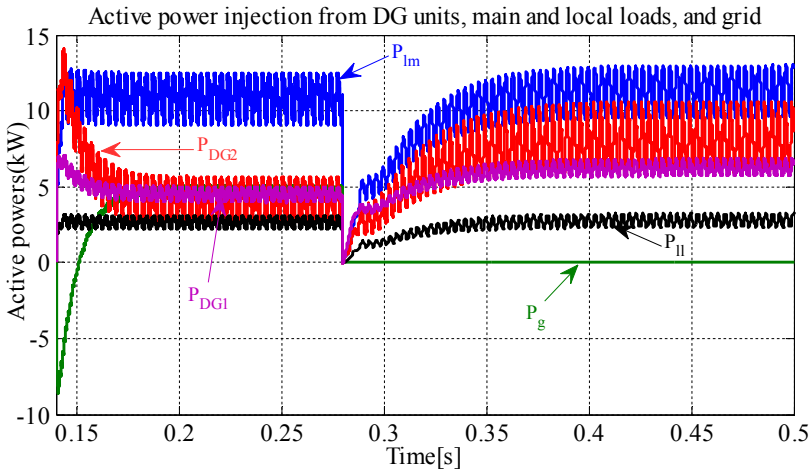

Fig. 15. The active power sharing between the main and local loads, grid, and DG units during the conversion from grid-connected mode to the islanded mode.

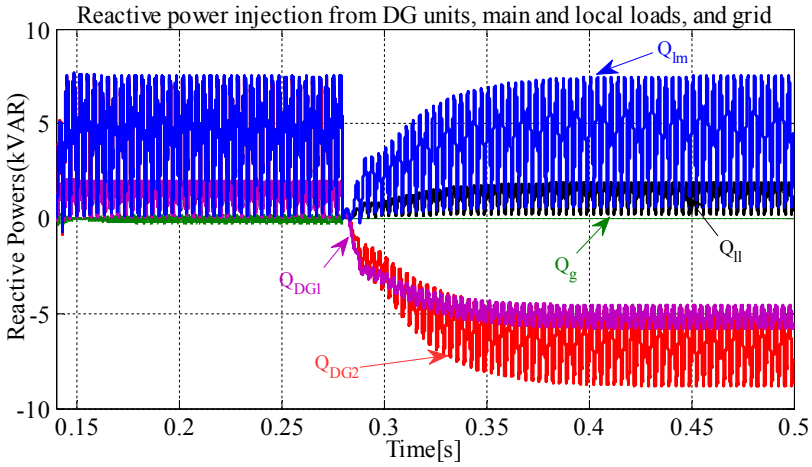

Fig. 16. The reactive power sharing between the main and local loads, grid, and DG units during the conversion from grid-connected mode to the islanded mode.

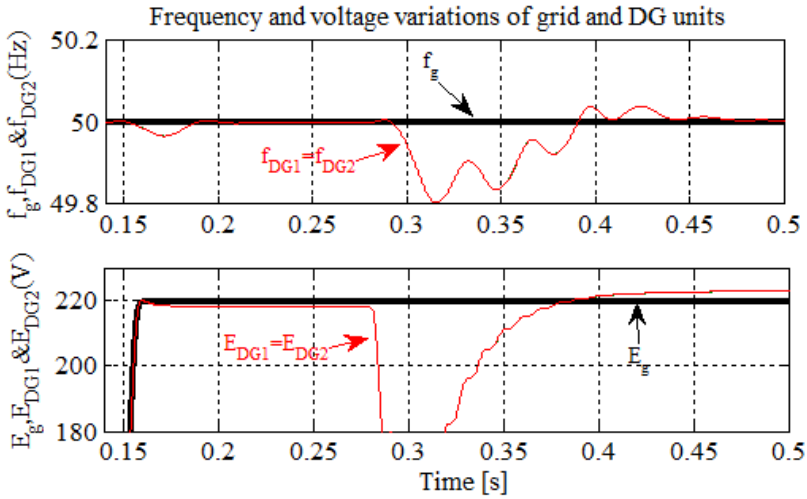

Fig. 17. Variations of frequency and voltage amplitude of the grid and DG units during the conversion from grid-connected mode to the islanded mode.

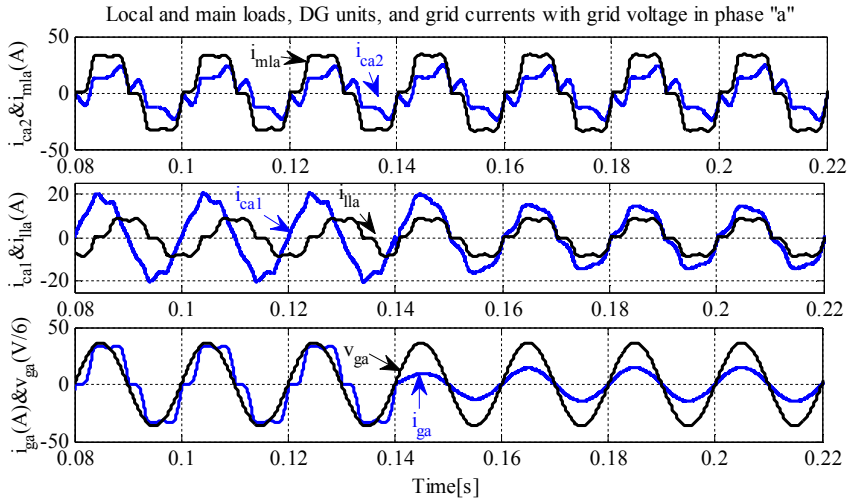

Fig. 18. Local and main loads, DG units, and grid currents with grid voltage in phase “a”.

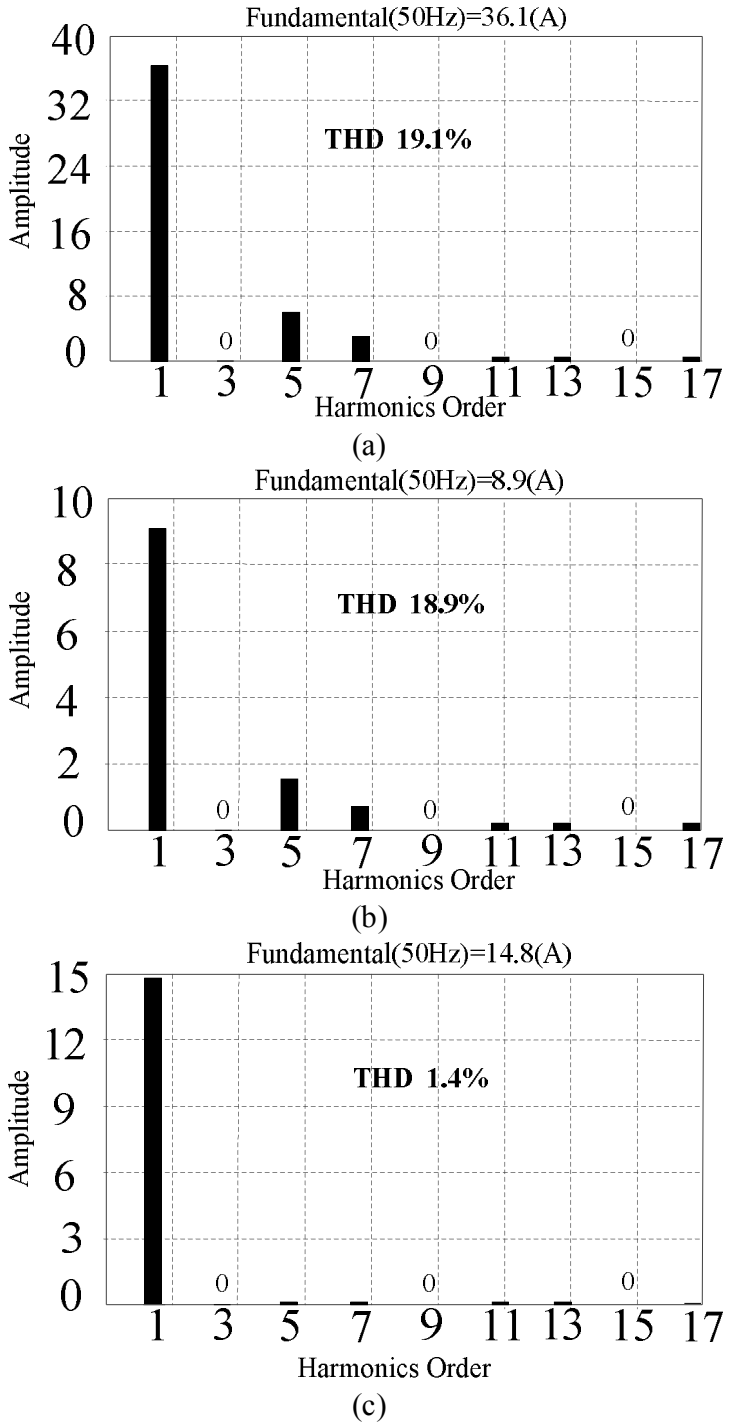

Fig. 19. Harmonic spectrum of, (a) Main load, (b) Local load, and (c) Grid currents in grid-connected mode, in phase "a".